J Neurophysiol 114: 2903–2911, 2015.
First published September 23, 2015; doi:10.1152/jn.00677.2015.

Optogenetic study of the projections from the bed nucleus of the stria terminalis to the central amygdala

Nur Zeynep Gungor, Ryo Yamamoto, and Denis Paré
Center for Molecular and Behavioral Neuroscience, Rutgers University-Newark, Newark, New Jersey

Submitted 8 July 2015; accepted in final form 21 September 2015

Gungor NZ, Yamamoto R, Paré D. Optogenetic study of the projections from the bed nucleus of the stria terminalis to the central amygdala. *J Neurophysiol* 114: 2903–2911, 2015. First published September 23, 2015; doi:10.1152/jn.00677.2015.—It has been proposed that the central amygdala (CeA), particularly its medial sector (CeM), generates brief fear responses to discrete conditioned cues, whereas the bed nucleus of the stria terminalis (BNST) promotes long-lasting, anxiety-like states in response to more diffuse contingencies. Although it is believed that BNST-CeA interactions determine the transition between short- and long-duration responses, the nature of these interactions remains unknown. To shed light on this question, we used a double viral strategy to drive the expression of channelrhodopsin (ChR2) in BNST cells that project to CeA. Next, using patch-clamp recordings in vitro, we investigated the connectivity of infected cells to noninfected cells in BNST and compared the influence of BNST axons on neurons in the medial and lateral (CeL) parts of CeA. CeA-projecting BNST cells were concentrated in the anterolateral (AL) and anteroventral (AV) sectors of BNST. Dense plexuses of BNST axons were observed throughout CeA. In CeA and BNST, light-evoked excitatory postsynaptic potentials accounted for a minority of responses (0–9% of tested cells); inhibition prevailed. The incidence of inhibitory responses was higher in CeM than in CeL (66% and 43% of tested cells, respectively). Within BNST, the connections from CeA-projecting to non-CeA-targeting cells varied as a function of the BNST sector: 50% vs. 9% of tested cells exhibited light-evoked responses in BNST-AL vs. BNST-AV, respectively. Overall, these results suggest that via its projection to CeA, BNST exerts an inhibitory influence over cued fear and that BNST neurons projecting to CeA form contrasting connections in different BNST subnuclei.

fear; anxiety; BNST; central amygdala

THE CENTRAL AMYGDALA (CeA) and bed nucleus of the stria terminalis (BNST) are thought to play different roles in the genesis of negative emotional states. For instance, lesion and inactivation studies have revealed that CeA, but not BNST (Duvarci et al. 2009; Hitchcock and Davis 1991; LeDoux et al. 1988; Walker and Davis 1997), is critically involved in the expression of conditioned fear responses to discrete sensory cues. On the other hand, BNST lesions decrease light-enhanced startle (Walker and Davis 1997) and contextual fear (Duvarci et al. 2009; Sullivan et al. 2004), leading to the hypothesis that BNST generates prolonged anxiety-like states in response to more diffuse contingencies (Walker et al. 2009).

The properties that support the differing contributions of CeA and BNST to fear and anxiety are unknown. Indeed, their connectivity is nearly identical. For instance, BNST and CeA target the same brain stem structures (Holstege et al. 1985; Hopkins and Holstege 1978), including those known to generate the behavioral (e.g., periaqueductal gray) and cardiovascular correlates (e.g., dorsal vagal nucleus and nucleus tractus solitarii) of negative emotional states. Moreover, they both receive glutamatergic inputs from the basolateral amygdala (BLA; Dong et al. 2001a; Krettek and Price 1978; Pare et al. 1995), midline thalamic nuclei (Vertes et al. 2015), and a similar array of cortical regions (McDonald et al. 1999). However, BNST projects to the paraventricular hypothalamic nucleus, whereas CeA does not (Dong et al. 2001b; Dong and Swanson 2006; Prewitt and Herman 1998).

Given that BNST and CeA receive similar inputs and mostly target the same structures, what explains their differing contributions to the genesis of negative emotional states? It was proposed that direct interactions between BNST and CeA might be involved (Walker et al. 2009). In support of this possibility, CeA sends strong GABAergic projections to BNST (Shin et al. 2008; Sun and Cassell 1993; Weller and Smith 1982), and optogenetic activation of these projections elicits inhibitory postsynaptic potentials (IPSPs) in target BNST cells (Li et al. 2012). BNST, particularly its anterolateral (BNST-AL) and anteroventral (BNST-AV) sectors, projects back to CeA (Dong et al. 2001b; Dong and Swanson 2004; Sun and Cassell 1993), and inhibition of BNST with muscimol infusions enhances conditioned fear to cues (Meloni et al. 2006). BNST projections to CeA are strongest to its medial sector (CeM) and lighter to its lateral part (CeL) (Dong et al. 2001b; Sun and Cassell 1993).

At present, it is unclear how BNST influences CeA, in part because the neurotransmitter used by CeA-projecting BNST cells has not been identified. Although most BNST neurons are GABAergic, some glutamatergic cells are also present, especially in BNST-AV (Poulin et al. 2009), and little is known about their projection sites. Thus, to shed light on the impact of BNST inputs on CeA, we used a double viral strategy to selectively drive the expression of channelrhodopsin (ChR2) in BNST cells that project to CeA. Using whole cell patch-clamp recordings in vitro, we then investigated the influence of BNST on CeA neurons and assessed the connectivity of infected to noninfected BNST cells.

MATERIALS AND METHODS

Animals and virus injections. Procedures were approved by the Institutional Animal Care and Use Committee of Rutgers University, in compliance with the Department of Health and Human Services *Guide for the Care and Use of Laboratory Animals*. Male Lewis rats (225–250 g) were anesthetized with a mixture of isoflurane and oxygen and placed into a stereotaxic apparatus. Body temperature was kept at 37–38°C. Atropine methyl nitrate (0.05 mg/kg im) was administered to aid breathing. Betadine and alcohol was used to clean

Address for reprint requests and other correspondence: D. Paré, Center for Molecular and Behavioral Neuroscience, Rutgers State Univ., 197 Univ. Ave., Newark, NJ 07102 (e-mail: pare@andromeda.rutgers.edu).

the scalp. Bupivacaine was injected in the region to be incised (0.125% solution, sc). Small burr holes were drilled above BNST (in mm, relative to bregma: AP: −0.36, ML: −1.6, DV: 6.8 and 7.4) and CeA (AP: −2.4, ML: 4.2, DV: 8.2 and 8.4). Nanoject II (Drummond Scientific) was used to make pressure injections (1 μl total; 0.5 μl at each DV level) at a rate of 9.6 nl/5 s using glass pipettes pulled to an outer tip diameter of ~70 μm by a PE-22 puller (Narishige Instruments).

EF1a-DIO-hChR2(H134R)-EYFP was infused in BNST and EF1a-mCherry-IRES-WGA-Cre in CeA (Fig. 1*A*). Adeno-associated virus serotype 5 was used for both viruses. In the second virus, Cre recombinase is fused to the transcellular tracer protein wheat germ agglutinin (WGA), which is retrogradely transported from CeA, to neurons that project to CeA. The first virus (infused in BNST) drives the expression of ChR2 and enhanced yellow florescence protein (EYFP), but only in cells that express Cre, because they project to CeA. These viruses were obtained from University of North Carolina Vector Core (Chapel Hill, NC). After the injections, the scalp was sutured, a local antibiotic (Neosporin paste) was applied on the wound, and an analgesic was administered (ketoprofen, 2 mg/kg sc twice a day for 3 days). Rats were used for in vitro experiments 6 wk after the virus injections because pilot experiments had revealed that this survival time was optimal for high transgene expression.

Slice preparation. Rats were anesthetized with avertin (300 mg/kg ip), followed by isoflurane. After abolition of reflexes, they were perfused with an ice-cold solution containing (in mM) 126 choline chloride, 2.5 KCl, 1 $MgCl_2$, 26 $NaHCO_3$, 1.25 NaH_2PO_4, 2 $CaCl_2$, and 10 glucose. The brains were sliced with a vibrating microtome (350-μm thickness) while submerged in the same solution. The slices were then kept in an oxygenated chamber containing the same solution as above except for the substitution of 126 mM NaCl for choline chloride (pH 7.3, 300 mOsm). The temperature of the chamber was kept at 34°C for 20 min and then returned to room temperature. One hour later, a first slice was transferred to the recording chamber perfused with the latter oxygenated solution at 32°C (6 ml/min).

Electrophysiology. First, using fluorescence microscopy (Axio Scope; Zeiss), we verified the location of the injection sites. A CeA injection site was considered accurate when mCherry expression covered the entire CeA and did not spread to the neighboring BLA or medial amygdala. A BNST injection was considered accurate when EYFP expression was present in BNST and absent from adjacent structures. We defined BNST-AL as the lateral area above the anterior commissure, which corresponds to the oval, juxtacapsular, and anterolateral subnuclei in the nomenclature of Ju and Swanson (1989). We defined BNST-AV as all the BNST subnuclei located below the anterior commissure. Data from a particular animal were only considered when the injection sites met the above criteria and at least one responsive cell was recorded.

Whole cell recordings were obtained under visual guidance using infrared differential interface contrast microscopy. We used 5- to 8-MΩ pipettes pulled from borosilicate glass capillaries. The intracellular solution contained (in mM) 130 K-gluconate, 10 HEPES, 10 KCl, 2 $MgCl_2$, 2 ATP-Mg, and 0.2 GTP-Tris (pH 7.2, 280 mOsm). The liquid junction potential was 10 mV with this solution. However, the membrane potential values mentioned below were not corrected for the junction potential. We used a MultiClamp 700B Amplifier (Molecular Devices) and digitized the data at 10 kHz with a Digidata 1550 interface controlled by pCLAMP version 10.3 (Molecular Devices).

To characterize the electroresponsive properties of the cells, we applied graded series of current pulses (±10-pA increments, 500 ms, 0.2 Hz). The input resistance of the cells was calculated from the voltage response to the lowest current injection. Blue light stimulation was provided by a 200- to 230-μm optic fiber patch cable coupled to a PlexBright tabletop blue LED module (Plexon, Dallas, TX). The light power density at the tip of the fibers was ~700 mW/mm^2. The distance between the recording pipette and the fiber optic tip was ~200 μm. Postsynaptic potentials or currents were evoked from several membrane potentials. The IPSP or inhibitory postsynaptic current (IPSC) reversal potentials were calculated from the linear fit of fluctuations in IPSP or IPSC amplitudes as a function of membrane potential. Picrotoxin, 6-cyano-7-nitroquinoxaline-2,3-dione disodium salt (CNQX), and ±-3-(2-carboxypiperazin-4-yl)propyl-1-phosphonic acid (CPP) were used for abolishing $GABA_A$, AMPA, and NMDA-dependent responses respectively. All drugs were obtained from Sigma (St. Louis, MO).

Blue light stimuli (2 or 5 ms) were generally applied at 0.05, 1, or 5 Hz. This range of stimulation frequencies was selected for the following reasons. First, we previously observed that most BNST-AL and BNST-AM (anteromedial) neurons fire at low rates in awake freely moving rats: around 85% of the cells fired below 4 Hz, and the group average was around 2–3 Hz (Haufler et al. 2013). Second, we aimed to minimize use-dependent depression of optogenetically elicited synaptic responses, a phenomenon observed frequently at higher stimulation frequencies. However, given that the light-evoked PSPs we observed generally lasted <0.2 s and that BNST cells fire at low rates (Haufler et al. 2013), it is unlikely that the PSPs elicited by a single BNST axon undergo temporal summation during baseline activity. However, summation of PSPs generated by different input neurons on a common target most likely occurs.

Imaging. Immediately after the recordings, in vitro slices were fixed in 4% paraformaldehyde for 12 h. The slices were then examined with Stereo Investigator v11 software (MBF Biosciences) and Nikon Eclipse E800. The boundaries of BNST and CeA were drawn on the brightfield images. The fluorescence images were superimposed on the brightfield images to assess virus diffusion. Confocal images were taken using Olympus FluoView FV1000 and FV10-ASW v3 software. Four *z* steps of 1.16 μm were collapsed to create the image stacks.

Statistics. We used Fisher exact tests to compare the incidence of responsive cells in different subnuclei. Unpaired *t*-tests were used to assess significance of differences between the electrophysiological properties of responsive and unresponsive cells.

RESULTS

Approach and database. We used a dual viral strategy to drive the expression of ChR2 and EYFP in BNST neurons that project to CeA (Fig. 1). To this end, EF1a-mCherry-IRES-WGA-Cre was infused in CeA (Fig. 1*A1*, red), causing the expression of Cre in neurons projecting to CeA. EF1a-DIO-hChR2(H134R)-EYFP was infused in BNST (Fig. 1*A1*, green), causing the expression of ChR2 and EYFP, but only in Cre-expressing BNST neurons. Six weeks after the virus infusions, coronal slices of the amygdala (Fig. 1*A2*) and BNST (Fig. 1*A3*) were prepared for whole cell patch-clamp recordings. Electrophysiological recordings from 13 animals are included in this data set. Two rats were used for anatomical observations only. Seven additional animals were excluded because of improper location of the virus injections. We obtained stable whole cell recordings from 34 BNST-AL (4 $EYFP^+$ and 30 $EYFP^-$), 37 BNST-AV (3 $EYFP^+$ and 34 $EYFP^-$), 28 CeL, and 23 CeM neurons.

The physiological properties of BNST and CeA neurons did not appear to have been altered by the dual viral strategy, because they matched earlier descriptions from this and other laboratories (BNST: Hammack et al. 2007; Rodriguez-Sierra et al. 2013; CeA: Amano et al. 2012; Dumont et al. 2002; Lopez De Armentia and Sah 2004). Specifically, consistent with prior reports, in both BNST-AL and AV, fast inward rectifying (fIR) cells were rare (7% and 9% of recorded cells, respectively).

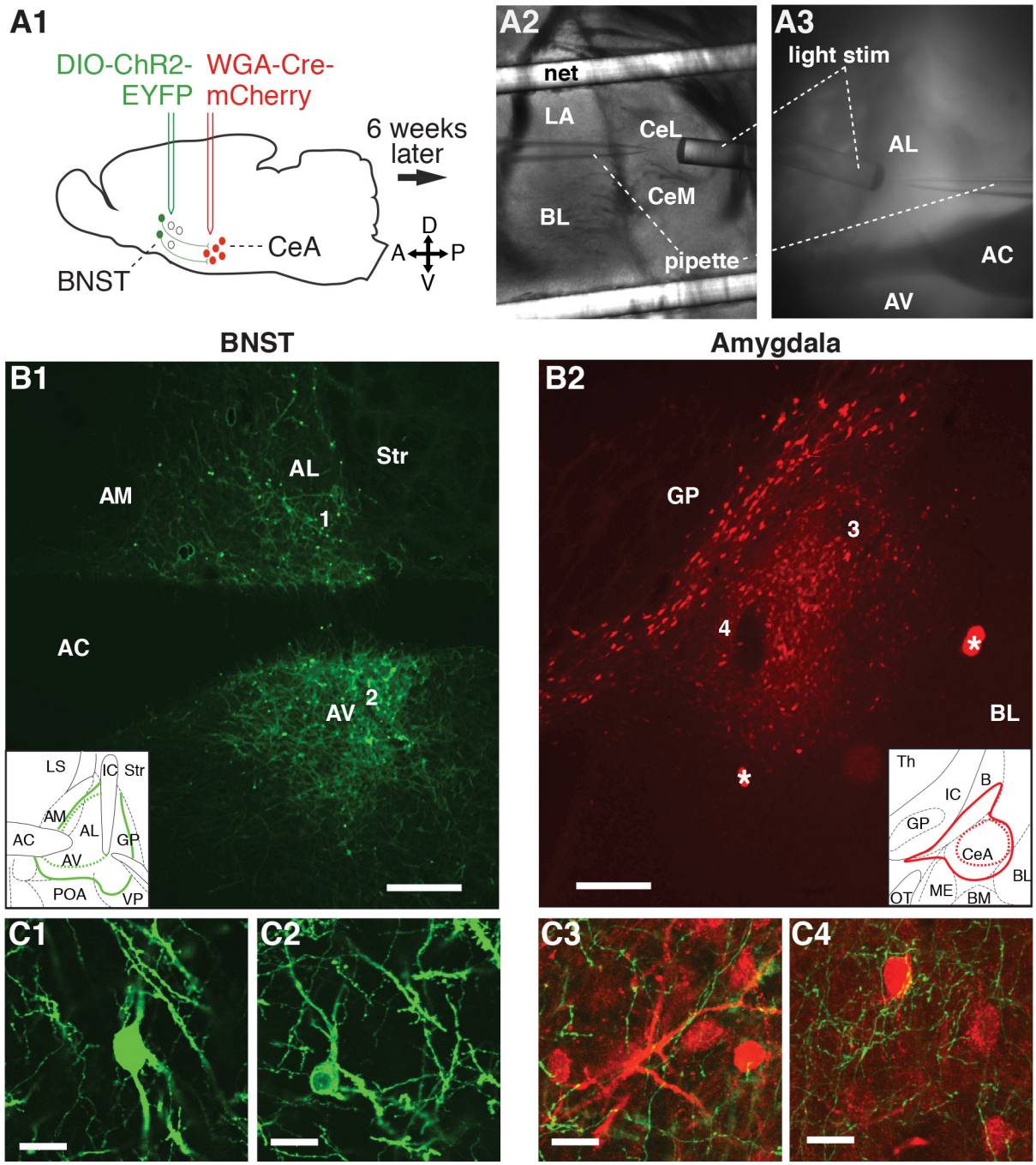

Fig. 1. *A*: experimental design. *A1*: dual viral strategy for selectively driving channelrhodopsin (ChR2) expression in neurons of the bed nucleus of the stria terminalis (BNST) that project to the central amygdala. Six weeks after the virus infusions, coronal slices of the amygdala (*A2*) and BNST (*A3*) were prepared for whole cell patch-clamp recordings. Blue light stimuli (light stim) were applied through optic fibers positioned at proximity of the recorded cells. We studied the impact of inputs from the central nucleus of the amygdala (CeA)-projecting BNST neurons onto CeA cells and other BNST cells that do not project to CeA. *B1*: enhanced yellow fluorescent protein (EYFP)- and ChR2-expressing BNST neurons that project to CeA. *B2*: amygdala neurons expressing mCherry. *Insets* in *B1* and *B2* indicate the largest (solid colored lines) and smallest (dashed colored lines) region containing cells expressing EYFP and ChR2 (green) or mCherry (red), respectively. The numbers 1–4 in *B1* and *B2* mark the approximate location of the higher power pictures provided in *C1–C4*, respectively. *C1* and *C2*: $EYFP^+$ BNST cells. *C3* and *C4*: $EYFP^+$ BNST axons (green) in close proximity to mCherry+ CeA neurons (red). Scale bars in *B* and *C* correspond to 300 and 20 μm, respectively. Asterisks in *B2* mark artifacts. AC, anterior commissure; AL, anterolateral sector of BNST; AM, anteromedial sector of BNST; AV, anteroventral sector of BNST; B, nucleus basalis; BL, basolateral nucleus of the amygdala; BM, basomedial nucleus of the amygdala; CeL, lateral sector of CeA; CeM, medial sector of CeA; GP, globus pallidus; IC, internal capsule; LA, lateral septum; OT, optic tract; POA, preoptic area; Th, thalamus; Str, striatum; VP, ventral pallidum.

Regular spiking (RS; AL: 57%, AV: 38%) and low-threshold bursting (LTB; AL: 37%, AV: 53%) cells prevailed in both BNST sectors, as previously reported (Hammack et al. 2007; Rodriguez-Sierra et al. 2013).

In CeA, we observed LTB, RS, and late-firing (LF) cells, as reported previously. In CeM, most cells were LTB (43%) and RS (39%) neurons; LF cells accounted for a minority of the recordings (17%). These numbers match the proportions seen

in an earlier report in rats (Dumont et al. 2002). Also consistent with prior reports, in CeL there was a higher incidence of RS (43%) cells than LTB (10%) neurons. However, there was a higher incidence of LF cells (46%) in our sample compared with that reported in two prior studies (Amano et al. 2012; Dumont et al. 2002;). However, another study (Lopez De Armentia and Sah 2004) also reported a higher incidence of this cell type in CeL.

Anatomical observations. Figure 1 provides representative examples of the distribution of $EYFP^+$ neurons in BNST (Fig. 1*B1*) and of mCherry in CeA (Fig. 1*B2*). Higher power illustrations of labeled elements are provided in Fig. 1*C*. In all animals with successful injections ($n = 15$), we observed that BNST-to-CeA connections originated from BNST-AL and BNST-AV. Invariably, very few $EYFP^+$ cells were observed in BNST-AM. In the amygdala, $EYFP^+$ axons were observed throughout CeA (Fig. 1, *C3* and *C4*). These observations are consistent with prior tracing studies (Dong et al. 2001b; Sun and Cassell 1993).

Local BNST connections. With the methods we used, BNST cells that project to CeA express EYFP and ChR2 (Fig. 1, *B*, *C1*, and *C2*). $EYFP^-$ cells are assumed not to contribute projections to CeA. We first verified whether blue light stimuli could elicit firing in $EYFP^+$ cells. As expected, blue light stimuli (5 ms) reliably elicited spiking in all tested $EYFP^+$ cells (Fig. 2*A*, $n = 7$). Trains of blue light stimuli (40-Hz train of 5-ms light stimuli for 1 s) elicited spiking that persisted for the duration of the train (Fig. 2*A1*). In response to isolated light stimuli (5 ms at 2 Hz), all $EYFP^+$ cells generated action potentials, either single spikes, spike doublets, or high-frequency spike bursts (4–5 spikes at 150–300 Hz, Fig. 2*A2*; 2, 2, and 3 of 7 tested cells, respectively).

Although none of the tested $EYFP^-$ BNST cells ($n = 64$) showed light-evoked spiking, many showed subthreshold synaptic responses (Fig. 2*B*). In BNST-AL, 15 of 30 tested $EYFP^-$ cells responded to blue light stimulation (Fig. 3*A*), implying they receive inputs from the BNST cells that project to CeA. In 13 of these cells, blue light stimuli elicited IPSPs (Fig. 2*B1*); only 2 cells with excitatory responses were observed (Figs. 2*B2* and 3*A*). In BNST-AV, only 3 of 34 cells were responsive, and all of these had inhibitory responses (Fig. 3*B*). The proportion of responsive $EYFP^-$ cells was significantly lower in

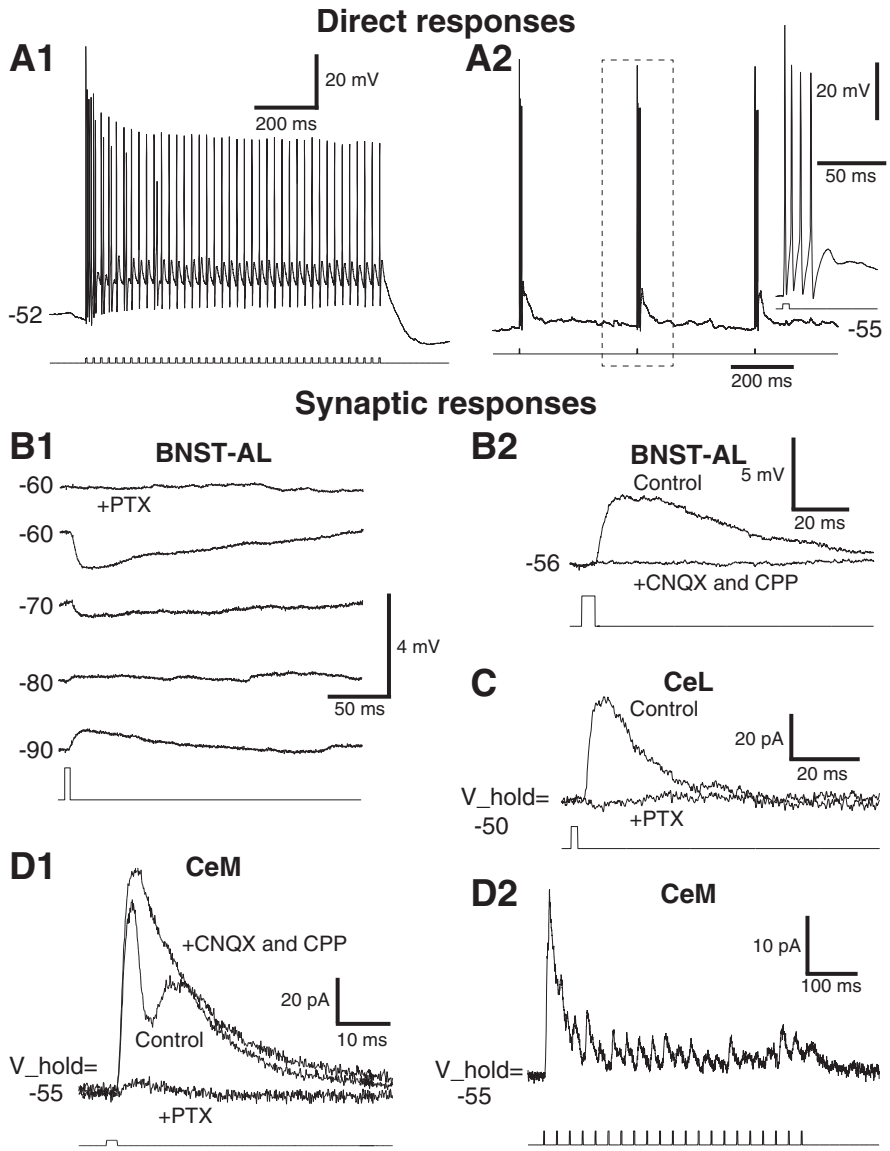

Fig. 2. Blue light evoked responses in BNST and CeA neurons. *A*: direct responses in ChR2-expressing BNST neurons that project to CeA. *A1*: train of light stimuli (*bottom*) reliably eliciting spikes (*top*). *A2*: at a lower frequency, each light stimulus (*bottom*) elicits a spike burst (*top*). *Inset* at *right* illustrates a light-evoked spike bursts with an expanded time base. *B*: examples of light-evoked responses in 2 different $EYFP^-$ BNST-AL neurons. *B1*: light-evoked activation of CeA-projecting BNST axons elicited inhibitory postsynaptic potentials (IPSPs) in a BNST-AL cell. Responses were elicited from different membrane potentials (numbers at *left*, in mV). Picrotoxin (PTX; 100 μM) application abolished the response (*top*) consistent with a mediation by $GABA_A$ receptors. *B2*: a rare case of light-evoked excitatory postsynaptic potential (EPSP; current-clamp mode). Light-evoked EPSP (Control) was abolished by addition of 6-cyano-7-nitroquinoxaline-2,3-dione disodium salt (CNQX;10 μM) and $\pm$-3-(2-carboxypiperazin-4-yl)propyl-1-phosphonic acid (CPP; 10 μM). *C*: example of light-evoked responses in a CeL neuron (voltage-clamp mode; holding potential $V\_hold = -50$ mV). Light-evoked IPSC (control) was abolished by PTX. *D*: examples of light-evoked responses in 2 different CeM neurons (voltage-clamp mode; $V\_hold = -55$ mV). *D1*: mixed excitatory-inhibitory response. Addition of CNQX and CPP to the perfusate abolished the EPSC. Subsequent application of picrotoxin almost completely abolished the residual response. *D2*: apparently pure inhibitory response to 40-Hz train of blue light stimuli. The response amplitude decreased during the train of light stimuli.

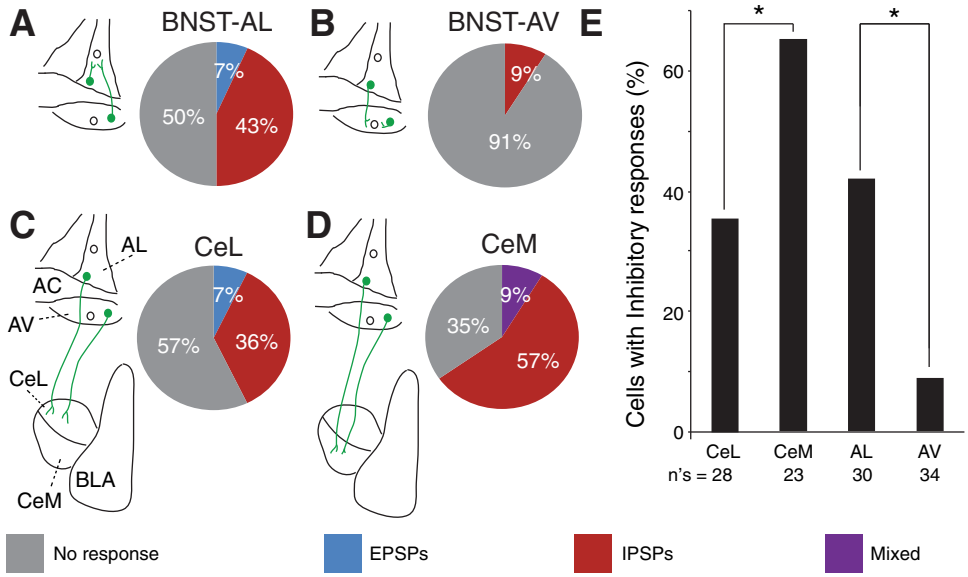

Fig. 3. Incidence and types of responses elicited by blue light stimuli in BNST-AL (*A*), BNST-AV (*B*), CeL (*C*), and CeM neurons (*D*). The schemes to the *left* of each pie chart illustrate the pathway stimulated and recording sites examined. In the pie charts, gray shading indicates the percentage of unresponsive cells, whereas red, blue, and purple indicate the percentages of neurons with IPSPs, EPSPs, or mixed responses, respectively. *E*: proportion of cells with inhibitory responses in the different regions examined.

BNST-AV than in BNST-AL (Fig. 3*E*; Fisher exact test, $P = 0.0003$). The leftmost two columns of Table 1 summarize the properties of the responses evoked in BNST-AL and AV neurons. Although the incidence of responses was markedly lower in BNST-AV than in BNST-AL, in both cases IPSP prevailed and exhibited similar properties, including a reversal potential around −77 mV.

Table 2 compares the electrophysiological properties of responsive and unresponsive cells in BNST-AL. At rheobase, responsive cells had a significantly longer firing latency than unresponsive cells [unpaired *t*-test, $t(28) = -2.87$, $P = 0.008$], despite having similar membrane time constant, input resistance, and spike threshold. This difference suggests that the distance between the soma and spike initiation zone is longer in responsive cells. In terms of the dynamics of current-evoked spiking, we observed no significant difference in the incidence of fIR, LTB, and RS cells between responsive and unresponsive cells [see Table 5; BNST-AL: $\chi^2(2, N = 30) = 4.29$, $P = 0.11$].

BNST inputs to CeA. Blue light stimulation of BNST axons evoked synaptic responses in 53% of tested CeA cells (CeL: 12 of 28, CeM: 15 of 23). Figure 2, *C* and *D*, depicts examples of light-evoked synaptic responses observed in CeL and CeM neurons, respectively. As in EYFP$^-$ BNST cells, most light-evoked responses were inhibitory in CeA cells (Figs. 2, *C* and *D2*, and 3, *C* and *D*). Excitatory responses were observed in only 4 of 51 tested CeA cells, and in 2 of these, they were superimposed on IPSPs or IPSCs (Fig. 2*D1*).

Consistent with prior tracing studies indicating that BNST projections are stronger to CeM than to CeL (Dong et al. 2001b; Sun and Cassell 1993), the incidence of CeA cells with inhibitory responses was significantly higher in CeM than in CeL (Fig. 3*E*; Fisher exact test, $P = 0.05$). However, compared with BNST neurons, light-evoked IPSPs had a significantly less negative reversal potential in CeA cells [CeA: −70.7 ± 1.8 mV; BNST: −78.2 ± 2.7 mV; unpaired *t*-test, $t(33) = 5.55$, $P = 0.02$], suggesting that chloride homeostatic mechanisms differ in the two cell types or that the light-activated inputs end more distally in the dendritic tree of BNST than CeA cells.

The two rightmost columns of Table 1 compare the properties of light-evoked responses in CeL and CeM neurons. In both regions, IPSPs were more frequent than excitatory postsynaptic potentials (EPSPs). IPSPs had a similar latency and reversal potential. Consistent with the higher incidence of inhibitory responses in CeM than CeL neurons, the amplitude of light-evoked IPSPs tended to be higher in CeM than CeL cells. However, the amplitude difference did not reach significance [unpaired *t*-test, $t(22) = 2.52$; $P = 0.13$].

Table 1. *Properties of light-evoked responses in BNST and CE neurons*

	BNST-AL	BNST-AV	CeL	CeM
IPSP incidence	13/30	3/34	10/28	15/23
IPSP latency, ms	4.31 ± 0.3	3.07 ± 0.9	5.51 ± 1.02	4.1 ± 0.58
IPSP amplitude, mV	−2.94 ± 0.52	−5.12 ± 3.07	−1.77 ± 0.38	−3.27 ± 0.75
IPSP reversal, mV*	−78.6 ± 3.3	−76.79 ± 2.9	−68.8 ± 1.4	−71.59 ± 2.54
EPSP incidence	2/30	0/34	2/28	2/23
EPSP latency, ms	7.27 ± 0.03	N/A	2.17 ± 0.03	4.08 ± 0.98
EPSP amplitude, mV	1.72 ± 0.74	N/A	2.8 ± 0.87	3.41 ± 1.35

Values are means ± SE for neurons in the anterolateral (AL) and anteroventral (AV) sectors of the bed nucleus of the stria terminalis (BNST) and in the lateral (CeL) and medial sectors of the central amygdala (CeM). EPSP and IPSP, excitatory and inhibitory postsynaptic potentials, respectively. *$P < 0.05$.

Table 2. *Physiological properties of responsive and nonresponsive BNST-AL neurons*

	Responsive Cells	Nonresponsive Cells	*P* Value
Resting potential, mV	−62.9 ± 2.4	−62.5 ± 1.9	0.91
Input resistance, MΩ	706.9 ± 51.3	658.3 ± 50.6	0.5
Time constant, ms	46.9 ± 5.3	51.6 ± 6.9	0.6
Rheobase, pA	15.3 ± 2.4	18.7 ± 2.2	0.31
Spike threshold, mV	−43.1 ± 1.1	−45.5 ± 1.7	0.24
Spike latency, ms	94.7 ± 12.6	50 ± 9.2	0.008*
Spike amplitude, mV	81.4 ± 4.3	78.2 ± 3.9	0.59
Spike duration at half-amplitude, ms	0.62 ± 0.06	0.69 ± 0.06	0.41
Firing rate at rheobase, Hz	5.1 ± 0.7	4.7 ± 0.7	0.69

Values are means ± SE for responsive ($n = 15$) and nonresponsive ($n = 15$) BNST-AL neurons. *$P < 0.05$.

Table 3. *Physiological properties of responsive and nonresponsive CeL neurons*

	Responsive Cells	Nonresponsive Cells	*P* Value
Resting potential, mV	−62.3 ± 2.3	−61.4 ± 1.1	0.72
Input resistance, MΩ	506.2 ± 84.5	413.4 ± 26.8	0.25
Time constant, ms	60 ± 6.9	54.8 ± 5.5	0.56
Rheobase, pA	35 ± 8.2	33.1 ± 3.4	0.82
Spike threshold, mV	−43.2 ± 0.9	−42.8 ± 1	0.81
Spike latency, ms	67.6 ± 14.6	118.8 ± 28	0.15
Spike amplitude, mV	94.1 ± 2.2	89.5 ± 2	0.13
Spike duration at half-amplitude, ms	0.6 ± 0.05	0.56 ± 0.04	0.7
Firing rate at rheobase, Hz	6.8 ± 0.7	7.6 ± 1.3	0.64

Values are means ± SE for responsive ($n = 12$) and nonresponsive CeL neurons ($n = 16$).

To test whether BNST axons target a specific subset of CeA cells, we compared the physiological properties of responsive and unresponsive CeA cells (CeL, Table 3; CeM, Table 4). In both sectors of CeA, no differences were observed between responsive and unresponsive neurons. This statement was true of their passive properties, the amplitude and duration of their action potentials, or the dynamics of current-evoked spiking. With respect to the latter point, we observed no significant differences in the incidence of RS, LTB, and LF cells (Table 5) between responsive and unresponsive CeL [$\chi^2(2, N = 28) = 0.8$, $P = 0.67$] or CeM neurons [$\chi^2(2, N = 23) = 2.84$, $P = 0.24$].

Last, we tested the pharmacological sensitivity of light-evoked synaptic responses in nine cells (Fig. 2, *B* and *C*). Irrespective of the recording site, all inhibitory responses were abolished or nearly obliterated by picrotoxin (100 μM; $n = 7$), whereas excitatory responses were eliminated or largely reduced by CNQX and CPP (both 10 μM; $n = 2$).

DISCUSSION

This study examined the physiology of BNST projections to CeA. The significance of this question stems from behavioral studies indicating that BNST and CeA play different roles in negative emotional states and the hypothesis that direct interactions between them explain their differing functions. Overall, we found that BNST exerts a prevalently inhibitory influence over CeA and that BNST neurons projecting to CeA form contrasting intrinsic connections in different BNST subnuclei. Below, we consider the significance of these findings in light of previous studies about the regulation of fear and anxiety.

Impact of BNST inputs on CeA neurons. Prior tracing studies indicated that BNST projections to CeA mainly originate in BNST-AL and BNST-AV (Dong et al. 2001b; Sun and Cassell 1993). Replicating these findings, our dual viral strategy led to strong EYFP expression in numerous BNST-AL and -AV neurons but in very few BNST-AM cells. Earlier studies also noted that the majority of BNST neurons are GABAergic (Cullinan et al. 1993; Polston et al. 2004; Poulin et al. 2009) and that BNST projections are denser to CeM than to CeL (Dong et al. 2001b). Consistent with this, we found that activation of BNST axons typically elicited inhibitory responses in CeA neurons and that their incidence was higher in CeM than in CeL.

However, CeM also receives GABAergic projections from CeL (Pitkänen et al. 1997), raising the possibility that, via CeL, BNST disinhibits CeM, opposing the inhibitory influence exerted by direct BNST inputs. A possible solution to this conundrum comes from recent reports indicating that different subsets of CeL neurons reciprocally inhibit each other and form contrasting connections with CeM (Ciocchi et al. 2010; Haubensak et al. 2010; Li et al. 2013; Viviani et al. 2011). For instance, somatostatin-immunonegative (SOM^-) CeL cells send inhibitory projections to CeM, whereas SOM^+ neurons do not (Li et al. 2013). Although it is currently unclear whether BNST axons form differential connections with SOM^- and SOM^+ neurons, a preferential innervation of SOM^+ cells by BNST axons would, via the disinhibition of SOM^- cells, potentiate the impact of direct BNST projections to CeM (Fig. 4*A*).

Although GABAergic cells prevail in BNST, some glutamatergic cells are also present, mostly in BNST-AV (Poulin et al. 2009). However, there is little data on their projection site(s). Some target the ventral tegmental area (Georges and Aston-Jones 2001, 2002; Jennings et al. 2013; Kudo et al. 2012), but it remains unclear whether they also project to CeA, although earlier observations hinted at this possibility (Sun and Cassell 1993). Supporting this, we observed light-evoked glutamatergic responses in CeA cells, but their incidence was very low. Nevertheless, it is possible that GABAergic and glutamatergic BNST neurons are targeted by different inputs, allowing for their independent activation. In this context, it should be noted that optogenetic activation of glutamatergic or GABAergic BNST-AV neurons elicits anxiogenic or anxiolytic effects, respectively (Jennings et al. 2013). In light of the low incidence of EPSPs in BNST-CeA connections, it seems unlikely that the negative emotional states evoked by activation of glutamatergic BNST-AV cells depend on BNST-CeA connections.

Although optogenetic methods are well suited to characterize neuronal connections and their role in behavior, it has so far proved difficult to study neuropeptide release driven by opsin activation. Although the light-evoked responses we observed were abolished by ionotropic receptor antagonists, neurons in BNST-AL and CeL express many neuropeptides (Gray and Magnuson 1987, 1992; Woodhams et al. 1983) that likely modulate fast inhibitory and excitatory neurotransmission (Kash et al. 2015; McElligott and Winder 2009). For example, Francesconi et al. (2009) demonstrated that corticotropin-releasing factor (CRF) impaired the long-term potentiation of intrinsic excitability in juxtacapsular BNST-AL neurons, mimicking the consequences of drug withdrawal. This effect may

Table 4. *Physiological properties of responsive and nonresponsive CeM neurons*

	Responsive Cells	Nonresponsive Cells	*P* Value
Resting potential, mV	−62.8 ± 2.4	−64.38 ± 2.8	0.68
Input resistance, MΩ	486.3 ± 82.5	487.7 ± 67.6	0.99
Time constant, ms	53.5 ± 8.5	46.8 ± 14.9	0.67
Rheobase, pA	31.7 ± 5.8	37.1 ± 4.7	0.52
Spike threshold, mV	−42.3 ± 1.2	−42.6 ± 1.3	0.87
Spike latency, ms	108.3 ± 29.9	83.6 ± 35.5	0.61
Spike amplitude, mV	92.7 ± 2.2	96.4 ± 2.6	0.3
Spike duration at half-amplitude, ms	0.5 ± 0.03	0.42 ± 0.04	0.16
Firing rate at rheobase, Hz	4.8 ± 0.7	6 ± 1.9	0.5

Values are means ± SE for responsive ($n = 15$) and nonresponsive CeM neurons ($n = 8$).

Table 5. *Incidence of different physiological cell types among responsive and nonresponsive BNST and CeA neurons*

	RS			LTB			fIR		
	Total	r	nr	Total	r	nr	Total	r	nr
BNST-AL	17	11	6	11	4	7	2	0	2
BNST-AV	12	1	11	17	1	16	3	1	2
CeL	12	5	7	3	2	1	12	5	8
CeM	9	4	5	10	8	2	4	3	1

Values indicate incidence of responsive (r) and unresponsive (nr) BNST and CeA neurons. RS, regular spiking; LTB, low-threshold bursting; fIR, fast inward rectifying; LF, late firing.

lead to a reduced inhibitory control of CeA, contributing to the negative emotional state experienced during drug abstinence.

Implications for the regulation of fear and anxiety by the extended amygdala. It is widely accepted that CeM is the main output station of the amygdala for conditioned fear. Nearly all brain stem projections of the amygdala stem from CeM (Hopkins and Holstege 1978; Petrovich and Swanson 1997; Veening et al. 1984). In particular, CeM is the sole source of amygdala projections to the periaqueductal gray, which generates freezing (LeDoux et al. 1988), the most common index of conditioned fear. Moreover, CeM neurons fire at high rates during fear-inducing conditioned stimuli (Ciocchi et al. 2010; Duvarci et al. 2011), and optogenetic activation or inactivation of CeM triggers or impairs freezing, respectively (Ciocchi et al. 2010).

According to Walker et al. (2009), upon receiving threat signals from the BLA, CeM would immediately activate downstream brain stem effectors, generating brief fear reactions in response to discrete and short-lasting conditioned cues. By contrast, BNST activation, in addition to requiring BLA afferents, would depend on CRF inputs from CeL (Lee and Davis 1997; Sakana et al et al. 1986, 1987). Consequently, BNST would be activated more slowly and persistently, explaining its involvement in the generation of long-lasting anxiety-like states. This model also proposed that once activated, BNST inhibits CeM. In support of this, it was reported that intra-BNST infusion of muscimol enhanced cued conditioned fear (Meloni et al. 2006).

Whereas our findings are consistent with the idea that BNST inhibits CeM, how BNST also generates anxiety-like states is unclear. Indeed, at odds with the above model, activation of GABAergic BNST-AV cells induces place preference and anxiolytic effects (Jennings et al. 2013). The anxiolytic influence of BNST-AV extends to the negative regulation of the hypothalamic-pituitary-adrenal axis (Radley and Sawchenko 2011, 2015). Similarly, BNST-AL, which only contains GABAergic neurons, also suppresses fear and anxiety. For instance, BNST-AL stimulation reduces corticosterone levels (Dunn 1987), and BNST-AL lesions increase stress-induced gastric erosions (Henke 1984). Furthermore, most BNST-AL cells fire at higher rates in low compared with high fear states (Haufler et al. 2013). Last, CGRP infusions in BNST, which elicit anxiety-like responses, increase inhibitory tone in BNST-AL (Gungor and Pare 2014).

Overall, these results suggest that BNST-AL and the GABAergic cells of BNST-AV act as a fear/anxiety-suppressing system. Opposite to this, stimulation of BNST-AM increases circulating corticosterone levels (Dunn 1987), and most BNST-AM cells fire at higher rates in high compared with low fear states (Haufler et al. 2013). However, it is unclear how BNST-AM would promote fear and anxiety because it contributes sparse projections to the amygdala (Bienkowski and Rinaman 2013). A hypothalamic locus of action is possible (Gross and Canteras 2012) but remains to be tested.

One neglected point in the Walker et al. (1997) model is the importance of GABAergic CeA projections to BNST, which mainly arise from CeL and are especially dense in BNST-AL (Bienkowski and Rinaman 2013; Krettek and Price 1978; Sun et al. 1991; Sun and Cassell 1993; Weller and Smith 1982). A prior study reported that CeA axons elicit IPSPs in 81% of BNST-AL cells (Li et al. 2012), whereas we observed that 57% of CeM cells receive inhibitory inputs from BNST. Furthermore, we found that the GABA-A reversal potential was 8 mV more negative in BNST than CeA neurons. Given the higher incidence of inhibitory connections from CeA to BNST than in the opposite direction and the more negative reversal potential of IPSPs in BNST cells, it is likely that CeA gains the upper hand in reciprocal BNST-CeA interactions, determining the intensity of negative emotional responses (Fig. 4*B*).

BNST cells projecting to CeA form contrasting connections in different BNST subnuclei. In addition to BNST projections to CeA, our dual viral strategy presented us with the opportunity to examine the intrinsic BNST network. Indeed, EYFP-expressing (that is, CeA-projecting) neurons were intermingled with EYFP$^-$ (that is, non-CeA-projecting) cells, allowing us to study the connections from the former to the latter. Previously, a glutamate uncaging study had concluded that the intrinsic BNST-AL and AV networks were similar (Turesson et al. 2013). However, the projection sites of recorded cells were unidentified. Thus the null hypothesis in our experiments was that the connections formed by CeA-projecting neurons with

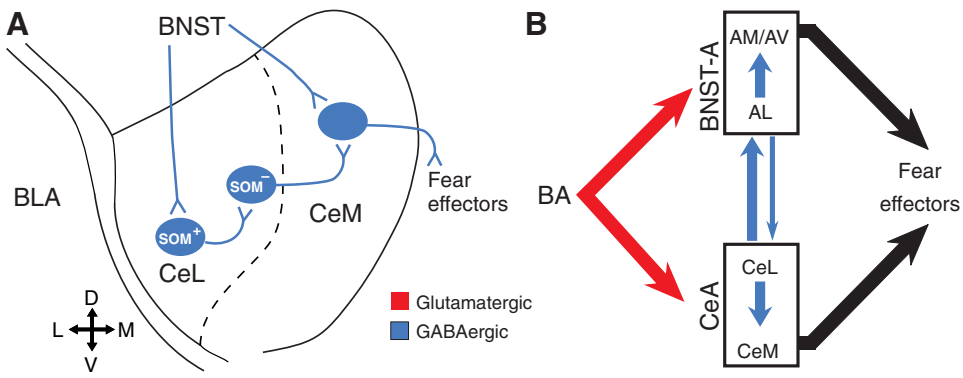

Fig. 4. Hypothetical schemes of BNST-CeA interactions. *A*: differential innervation of SOM$^+$ and SOM$^-$ CeL neurons by BNST axons. The direct inhibitory effects of BNST projections to CeM neurons are increased by the inhibition of SOM$^+$ CeL cells, leading to the disinhibition of SOM$^-$ CeL neurons. *B*: overall organization of the reciprocal BNST-CeA connections. SOM, somatostatin.

EYFP$^-$ cells would be similar in the two regions. In contrast, we observed a marked difference between the incidence of responsive EYFP$^-$ neurons in BNST-AL and -AV. In particular, activation of CeA-projecting cells elicited synaptic responses in 50% of EYFP$^-$ BNST-AL cells compared with 9% in BNST-AV. This is surprising given that the glutamate-uncaging study had found that projections from BNST-AL to -AV were stronger than in the opposite direction (Turesson et al. 2013). These results suggest that in BNST-AV at least, neurons with different projection sites form different intrinsic connections. A challenge for future studies will be to extend these analyses to other projection sites of BNST while considering the transmitter phenotype of the cells.

GRANTS

This work was supported by National Institute of Mental Health Grant R01 MH-098738 (to D. Paré).

DISCLOSURES

No conflicts of interest, financial or otherwise, are declared by the authors.

AUTHOR CONTRIBUTIONS

N.Z.G. and D.P. conception and design of research; N.Z.G. and R.Y. performed experiments; N.Z.G. and R.Y. analyzed data; N.Z.G., R.Y., and D.P. interpreted results of experiments; N.Z.G. and D.P. prepared figures; N.Z.G. and D.P. drafted manuscript; N.Z.G., R.Y., and D.P. edited and revised manuscript; N.Z.G., R.Y., and D.P. approved final version of manuscript.

REFERENCES

Amano T, Amir A, Goswami S, Paré D. Morphology, PKCδ expression, and synaptic responsiveness of different types of rat central lateral amygdala neurons. *J Neurophysiol* 108: 3196–3205, 2012.

Bienkowski MS, Rinaman L. Common and distinct neural inputs to the medial central nucleus of the amygdala and anterior ventrolateral bed nucleus of stria terminalis in rats. *Brain Struct Funct* 218: 187–208, 2013.

Ciocchi S, Herry C, Grenier F, Wolff SB, Letzkus JJ, Vlachos I, Ehrlich I, Sprengel R, Deisseroth K, Stadler MB, Müller C, Lüthi A. Encoding of conditioned fear in central amygdale inhibitory circuits. *Nature* 468: 270–276, 2010.

Cullinan WE, Herman JP, Watson SJ. Ventral subicular interaction with the hypothalamic paraventricular nucleus: evidence for a relay in the bed nucleus of the stria terminalis. *J Comp Neurol* 13: 1258–1279, 1993.

Dong HW, Petrovich GD, Swanson LW. Topography of projections from amygdala to bed nuclei of the stria terminalis. *Brain Res Brain Res Rev* 38: 192–246, 2001a.

Dong HW, Petrovich GD, Watts AG, Swanson LW. Basic organization of projections from the oval and fusiform nuclei of the bed nuclei of the stria terminalis in adult rat brain. *J Comp Neurol* 436: 430–455, 2001b.

Dong HW, Swanson LW. Organization of axonal projections from the anterolateral area of the bed nuclei of the stria terminalis. *J Comp Neurol* 468: 277–298, 2004.

Dong HW, Swanson LW. Projections from bed nuclei of the stria terminalis, anteromedial area: cerebral hemisphere integration of neuroendocrine, autonomic, and behavioral aspects of energy balance. *J Comp Neurol* 494: 142–178, 2006.

Dumont EC, Martina M, Samson RD, Drolet G, Paré D. Physiological properties of central amygdala neurons: species differences. *Eur J Neurosci* 15: 545–552, 2002.

Dunn JD. Plasma corticosterone responses to electrical stimulation of the bed nucleus of the stria terminalis. *Brain Res* 407: 327–331, 1987.

Duvarci S, Bauer EP, Paré D. The bed nucleus of the stria terminalis mediates inter-individual variations in anxiety and fear. *J Neurosci* 29: 10357–10361, 2009.

Duvarci S, Popa D, Paré D. Central amygdala activity during fear conditioning. *J Neurosci* 31: 289–294, 2011.

Francesconi W, Berton F, Koob GF, Sanna PP. Intrinsic neuronal plasticity in the juxtacapsular nucleus of the bed nucleus of the stria terminalis. *Prog Neuropsychopharmacol Biol Psychiatry* 33: 1347–1355, 2009.

Georges F, Aston-Jones G. Potent regulation of midbrain dopamine neurons by the bed nucleus of the stria terminalis. *J Neurosci* 21: RC160, 2001.

Georges F, Aston-Jones G. Activation of ventral tegmental area cells by the bed nucleus. *J Neurosci* 22: 5173–5187, 2002.

Gray TS, Magnuson DJ. Neuropeptide neuronal efferents from the bed nucleus of the stria terminalis and central amygdaloid nucleus to the dorsal vagal complex in the rat. *J Comp Neurol* 262: 365–374, 1987.

Gray TS, Magnuson DJ. Peptide immunoreactive neurons in the amygdala and the bed nucleus of the stria terminalis project to the midbrain central gray in the rat. *Peptides* 13: 451–460, 1992.

Gross CT, Canteras NS. The many paths to fear. *Nat Rev Neurosci* 13: 651–658, 2012.

Gungor NZ, Pare D. CGRP inhibits neurons of the bed nucleus of the stria terminalis: implications for the regulation of fear and anxiety. *J Neurosci* 34: 60–65, 2014.

Hammack SE, Mania I, Rainnie DG. Differential expression of intrinsic membrane currents in defined cell types of the anterolateral bed nucleus of the stria terminalis. *J Neurophysiol* 98: 638–656, 2007.

Haubensak W, Kunwar PS, Cai H, Ciocchi S, Wall NR, Ponnusamy R, Biag J, Dong HW, Deisseroth K, Callaway EM, Fanselow MS, Lüthi A, Anderson DJ. Genetic dissection of an amygdala microcircuit that gates conditioned fear. *Nature* 468: 270–276, 2010.

Haufler D, Nagy FZ, Pare D. Neuronal correlates of fear conditioning in the bed nucleus of the stria terminalis. *Learn Mem* 20: 633–641, 2013.

Henke PG. The bed nucleus of the stria terminalis and immobilization-stress: unit activity, escape behaviour, and gastric pathology in rats. *Behav Brain Res* 11: 35–45, 1984.

Hitchcock JM, Davis M. Efferent pathway of the amygdala involved in conditioned fear as measured with the fear-potentiated startle paradigm. *Behav Neurosci* 105: 826–842, 1991.

Holstege G, Meiners L, Tan K. Projections of the bed nucleus of the stria terminalis to the mesencephalon, pons, and medulla oblongata in the cat. *Exp Brain Res* 58: 379–391, 1985.

Hopkins DA, Holstege G. Amygdaloid projections to the mesencephalon, pons and medulla oblongata in the cat. *Exp Brain Res* 32: 529–547, 1978.

Jennings JH, Sparta DR, Stamatakis AM, Ung RL, Pleil KE, Kash TL, Stuber GD. Distinct extended amygdala circuits for divergent motivational states. *Nature* 496: 224–228, 2013.

Ju G, Swanson LW. Studies on the cellular architecture of the bed nuclei of the stria terminalis in the rat: I. Cytoarchitecture. *J Comp Neurol* 280: 587–602, 1989.

Kash TL, Pleil KE, Marcinkiewcv CA, Lowery-Gionta EG, Crowley N, Mazzone C, Sugam J, Hardaway JA, McElligott ZA. Neuropeptide regulation of signaling and behavior in the BNST. *Mol Cells* 38: 1–13, 2015.

Krettek JE, Price JL. Amygdaloid projections to subcortical structures within the basal forebrain and brainstem in the rat and cat. *J Comp Neurol* 178: 225–254, 1978.

Kudo T, Uchigashima M, Miyazaki T, Konno K, Yamasaki M, Yanagawa Y, Minami M, Watanabe M. Three types of neurochemical projection from the bed nucleus of the stria terminalis to the ventral tegmental area in adult mice. *J Neurosci* 32: 18035–18046, 2012.

LeDoux JE, Iwata J, Cicchetti P, Reis DJ. Different projections of the central amygdaloid nucleus mediate autonomic and behavioral correlates of conditioned fear. *J Neurosci* 8: 2517–2529, 1988.

Lee Y, Davis M. Role of hippocampus, the bed nucleus of the stria terminalis, and the amygdala in the excitatory effect of corticotropin-releasing hormone on acoustic startle reflex. *J Neurosci* 17: 6434–6446, 1997.

Li C, Pleil KE, Stamatakis AM, Busan S, Vong L, Lowell BB, Stuber GD, Kash TL. Presynaptic inhibition of gamma-aminobutyric acid release in the bed nucleus of the stria terminalis by kappa opioid receptor signaling. *Biol Psychiatry* 71: 725–732, 2012.

Li H, Penzo MA, Taniguchi H, Kopec CD, Huang ZJ, Li B. Experience-dependent modification of a central amygdala fear circuit. *Nat Neurosci* 16: 332–329, 2013.

Lopez De Armentia M, Sah P. Firing properties and connectivity of neurons in the rat lateral central nucleus of the amygdala. *J Neurophysiol* 92: 1285–1294, 2004.

McDonald AJ, Shammah-Lagnado SJ, Shi C, Davis M. Cortical afferents to the central extended amygdala. *Ann NY Acad Sci* 877: 309–338, 1999.

McElligott ZA, Winder DG. Modulation of glutamatergic synaptic transmission in the bed nucleus of the stria terminalis. *Prog Neuropsychopharmacol Biol Psychiatry* 33: 1329–1335, 2009.

Meloni EG, Jackson A, Gerety LP, Cohen BM, Carlezon WA Jr. Role of the bed nucleus of the stria terminalis (BST) in the expression of conditioned fear. *Ann NY Acad Sci* 1071: 538–541, 2006.

Paré D, Smith Y, Paré JF. Intra-amygdaloid projections of the basolateral and basomedial nuclei in the cat: *Phaseolus vulgaris*-leucoagglutinin anterograde tracing at the light and electron microscopic level. *Neuroscience* 69: 567–583, 1995.

Petrovich GD, Swanson LW. Projections from the lateral part of the central amygdalar nucleus to the postulated fear conditioning circuit. *Brain Res* 763: 247–254, 1997.

Pitkänen A, Savander V, LeDoux JE. Organization of intra-amygdaloid circuitries in the rat: an emerging framework for understanding functions of the amygdala. *Trends Neurosci* 20: 517–523, 1997.

Polston EK, Gu G, Simerly RB. Neurons in the principal nucleus of the bed nuclei of the stria terminalis provide a sexually dimorphic GABAergic input to the anteroventral periventricular nucleus of the hypothalamus. *Neuroscience* 123: 793–803, 2004.

Poulin JF, Arbour D, Laforest S, Drolet G. Neuroanatomical characterization of endogenous opioids in the bed nucleus of the stria terminalis. *Prog Neuropsychopharmacol Biol Psychiatry* 33: 1356–1365, 2009.

Prewitt CM, Herman JP. Anatomical interactions between the central amygdaloid nucleus and the hypothalamic paraventricular nucleus of the rat: a dual tract-tracing analysis. *J Chem Neuroanat* 15: 173–185, 1998.

Radley JJ, Sawchenko PE. A common substrate for prefrontal and hippocampal inhibition of the neuroendocrine stress response. *J Neurosci* 31: 9683–9695, 2011.

Radley JJ, Sawchenko PE. Evidence for involvement of a limbic paraventricular hypothalamic inhibitory network in hypothalamic-pituitary-adrenal axis adaptations to repeated stress. *J Comp Neurol* 523: 2769–2787, 2015.

Rodríguez-Sierra OE, Turesson HK, Pare D. Contrasting distribution of physiological cell types in different regions of the bed nucleus of the stria terminalis. *J Neurophysiol* 110: 2037–2049, 2013.

Sakana M, Shibasaki T, Lederis K. Distribution and efferent projections of corticotropin-releasing factor like immunoreactivity in the rat amygdaloid complex. *Brain Res* 382: 213–238, 1986.

Sakana M, Shibasaki T, Lederis K. Corticotropin releasing factor-like immunoreactivity in the rat brain as revealed by a modified cobalt-glucose oxidase-diaminobenzidine method. *J Comp Neurol* 260: 256–298, 1987.

Shin JW, Geerling JC, Loewy AD. Inputs to the ventrolateral bed nucleus of the stria terminalis. *J Comp Neurol* 511: 628–57, 2008.

Sullivan GM, Apergis J, Bush DEA, Johnson LR, Hou M, LeDoux JE. Lesions in the bed nucleus of the stria terminalis disrupt corticosterone and freezing responses elicited by a contextual but not by a specific cue-conditioned fear stimulus. *Neuroscience* 128: 7–14, 2004.

Sun N, Cassell MD. Intrinsic GABAergic neurons in the rat central extended amygdala. *J Comp Neurol* 330: 381–404, 1993.

Sun N, Roberts L, Cassell MD. Rat central amygdaloid nucleus projections to the bed nucleus of the stria terminalis. *Brain Res Bull* 27: 651–662, 1991.

Turesson HK, Rodriguez-Sierra O, Pare D. Intrinsic connections in the anterior part of the bed nucleus of the stria terminalis. *J Neurophysiol* 109: 2438–2450, 2013.

Veening JG, Swanson LW, Sawchenko PE. The organization of projections from the central nucleus of the amygdala to brainstem sites involved in central autonomic regulation: a combined retrograde transport-immunohistochemical study. *Brain Res* 303: 337–357, 1984.

Vertes RP, Linley SB, Hoover WB. Limbic circuitry of the midline thalamus. *Neurosci Biobehav Rev* 54: 89–107, 2015.

Viviani D, Charlet A, van den Burg E, Robinet C, Hurni N, Abatis M, Magara F, Stoop R. Oxytocin selectively gates fear responses through distinct outputs from the central amygdala. *Science* 333: 104–107, 2011.

Walker DL, Davis M. Double dissociation between the involvement of the bed nucleus of the stria terminalis and the central nucleus of the amygdala in light enhances versus fear-potentiated startle. *J Neurosci* 17: 9375–9383, 1997.

Walker DL, Miles LA, Davis M. Selective participation of the bed nucleus of the stria terminalis and CRF in sustained anxiety-like versus phasic fear-like responses. *Prog Neuropsychopharmacol Biol Psychiatry* 33: 1291–1308, 2009.

Weller KL, Smith DA. Afferent connections to the bed nucleus of the stria terminalis. *Brain Res* 232: 255–270, 1982.

Woodhams PL, Roberts GW, Polak JM, Crow TJ. Distribution of neuropeptides in the limbic system of the rat: the bed nucleus of the stria terminalis, septum and preoptic area. *Neuroscience* 8: 677–703, 1983.